ACS Catalysis

Research Article

pubs.acs.org/acscatalysis

Fibrous Nano-Silica Supported Ruthenium (KCC-1/Ru): A Sustainable Catalyst for the Hydrogenolysis of Alkanes with Good Catalytic Activity and Lifetime

Aziz Fihri, Mohamed Bouhrara, Umesh Patil, Dongkyu Cha, Youssef Saih, and Vivek Polshettiwar*

Nano-Catalysis Laboratory, KAUST Catalysis Centre (KCC), King Abdullah University of Science and Technology (KAUST), Thuwal 23955, Saudi Arabia

Supporting Information

ABSTRACT: We have shown that fibrous nanosilica (KCC-1) can serve as a suitable support for the synthesis of highly dispersed ruthenium (Ru) nanoparticles. The resulting KCC-1/Ru catalyst displayed superior activity for the hydrogenolysis of propane and ethane at atmospheric pressure and at low temperature. The high catalytic activity was due to the formation of Ru-nanoparticles with an active size range (1−4 nm) and the presence of hexagonal-shaped particles with several corners and sharp edges possessing reactive atoms with lowest coordination numbers. The catalyst was stable with an excellent lifetime and no sign of deactivation, even after eight days. This enhanced stability may be due to the fibrous nature of KCC-1 which restricts Ostwald ripening of Ru nanoparticles.

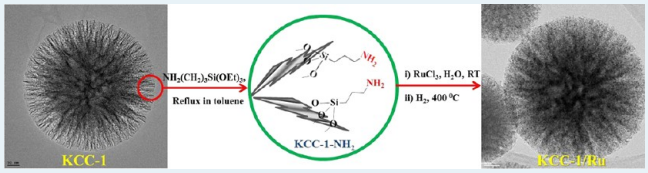

KEYWORDS: *fibrous nanosilica, nanocatalysis, ruthenium, hydrogenolysis, alkanes*

1. INTRODUCTION

Catalysis research has become one of the most powerful tools in the petrochemical and fine-chemical productions. Low-temperature skeletal cleavage and the making and breaking of carbon−carbon (C−C) bonds are of prime importance in the petrochemical industry as the transformation of crude oil into hydrocarbons is often necessary. In this regard, the hydrogenolysis of hydrocarbons, which is the cleavage of C−C bonds under hydrogen, is in increasing demand in petroleum processing. Hydrogenolysis is a major subset of reactions that occurs on supported transition-metal catalysts, which were first studied for ethane by Morikawa, Benedict, and Taylor.[1−3] John Sinfelt's research on hydrogenolysis had a tremendous impact on industrial catalysis systems for hydrogenolysis.[4−7] Metal-based catalysts including ruthenium-based have been extensively studied by Bond and others for the hydrogenolysis of alkanes and are some of the best catalysts for this reaction.[8−21]

Although a range of catalysts exists for the hydrogenolysis of alkanes,[1−21] two main challenges remain unresolved: (1) the stable nanocatalyst system that do not experience activity loss as the result of particle-size growth during the reaction because of Ostwald ripening and (2) nanocatalysts that are active at low temperatures and at atmospheric pressure and are also effective even for challenging substrates such as ethane.

In continuation of our quest for sustainable nanocatalytic protocols,[22−32] we herein report novel Ru nanocatalysts supported on our recently discovered high-surface-area silica with a unique fibrous morphology (KCC-1).[24−26] We observed that the high surface area of KCC-1 is attributable to fibers and not to pores, which dramatically increases its accessibility.[24] We believe that this unique property will be useful in the design of silica-supported catalysts, wherein the accessibility of active sites can be increased significantly. After recently demonstrating this concept for the hydro-metathesis of olefins using a KCC-1/TaH catalyst system,[25] and for Suzuki coupling reactions using KCC-1/Pd,[26] we designed a system of highly dispersed Ru nanoparticles supported on KCC-1 to examine the advantages of its fibrous nature, for the hydrogenolysis of propane and ethane.

2. EXPERIMENTAL SECTION

2.1. Preparation of KCC-1-NH_2. In a round-bottom flask, 150 mL of anhydrous toluene, 12 g of KCC-1, and 40 mL of 3-aminopropyltriethoxysilane (APTS) were introduced, and the mixture was refluxed for 48 h. The solution was filtered; the solid was washed with ethanol, and dried overnight at 65 °C under vacuum (0.075 mm of Hg) to yield the KCC-1-NH_2 nanocomposite.

2.2. Preparation of the KCC-1/Ru Nanocatalyst. A Schlenk flask was charged with 1 g of KCC-1-NH_2 material, 0.21 g of $RuCl_3$, and 50 mL of deionized water and then sonicated for 2 h. The mixture was vigorously stirred for 72 h at room temperature. The solid product was collected by centrifugation and washed several times with water, ethanol, and then dried under reduced pressure at 65 °C for 16 h. For the in situ preparation of the ruthenium nanoparticles, 200 mg of catalyst was placed in a stainless steel tubular reactor with a 9 mm internal diameter and was reduced in hydrogen flow (20

Received: March 18, 2012
Revised: June 4, 2012
Published: June 4, 2012

Scheme 1. Synthesis of KCC-1/Ru Nanocatalysts

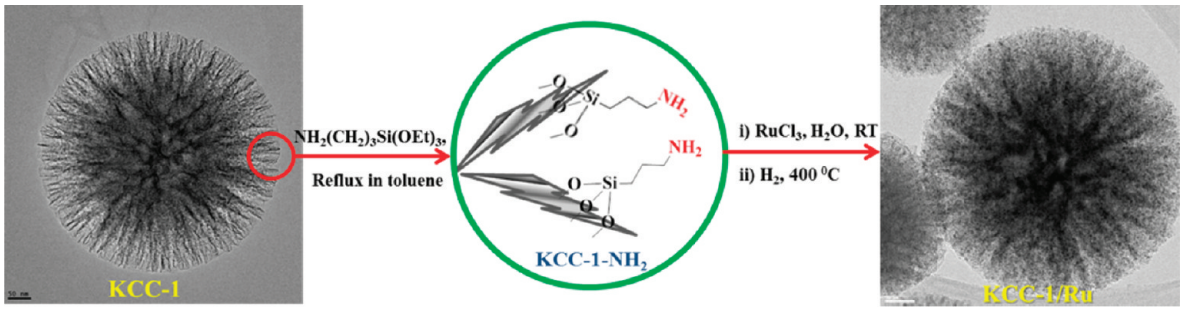

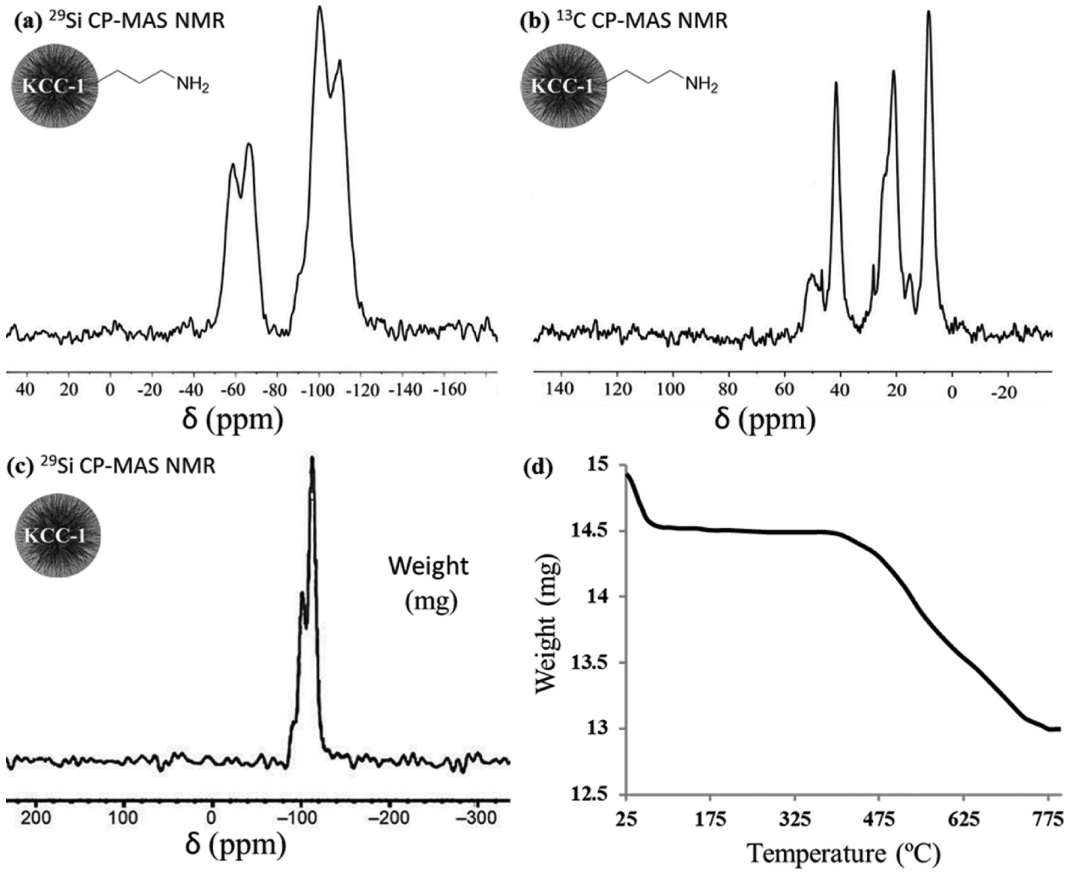

Figure 1. (a) ^{29}Si CP-MAS NMR spectrum of KCC-1-NH_2, (b) ^{13}C CP-MAS NMR spectrum of KCC-1-NH_2, (c) ^{29}Si CP-MAS NMR spectrum of KCC-1, (d) TGA thermogram of KCC-1-NH_2 in air.

mL/min) at 400 °C for 16 h. The ruthenium content of the final material (KCC-1/Ru) was determined by inductively coupled plasma-optical emission spectroscopy (ICP-OES) analysis and was found to be 7.11%.

2.3. Hydrogenolysis of Alkanes. The hydrogenolysis reactions of propane were conducted at 175 °C and at atmospheric pressure. A 200 mg portion of catalysts were placed in a fixed bed dynamic reactor in a continuous-flow of propane-H_2-He (1:4:20) at a total flow of 100 mL/min. The temperature of the reactor was controlled by a PID temperature controller connected to a thermocouple inserted in the catalyst bed. The flow of He, H_2, and propane were controlled by mass flow controllers, and the product gases were analyzed online with a Varian micro-GC CP-4900 using capillary columns (10 m PPU; 6 m 5CB; 10 m Al2) and FID detector. The hydrogenolysis reactions of ethane were carried out at 250 °C and at atmospheric pressure in the following flow rates: ethane (2 mL/min) and hydrogen (8 mL/min) using similar procedure as for propane.

2.4. TEM, TGA, and NMR Analysis. Transmission electron microscope (TEM) observations were performed on a FEI Titan operated at an accelerating voltage of 200 kV. For sample preparation, powders were dispersed in ethanol with the assistance of sonication, and one drop of the solution was dropped onto a carbon-coated TEM grid of 200 mesh. Thermo gravimetric analysis (TGA) was performed on a Mettler Toledo TGA/DSC1 Star apparatus. For analysis of aminopropyl loading, about 15 mg of KCC-1-NH_2 sample was heated in an alumina pan from ambient temperature to 800 °C at a heating rate of 5 °C/min under a 100 mL/min of air flow. All NMR experiments were conducted using a WB AVANCE III 600 MHz NMR spectrometer. The cross-polarization magic-

dx.doi.org/10.1021/cs300179q | ACS Catal. 2012, 2, 1425−1431

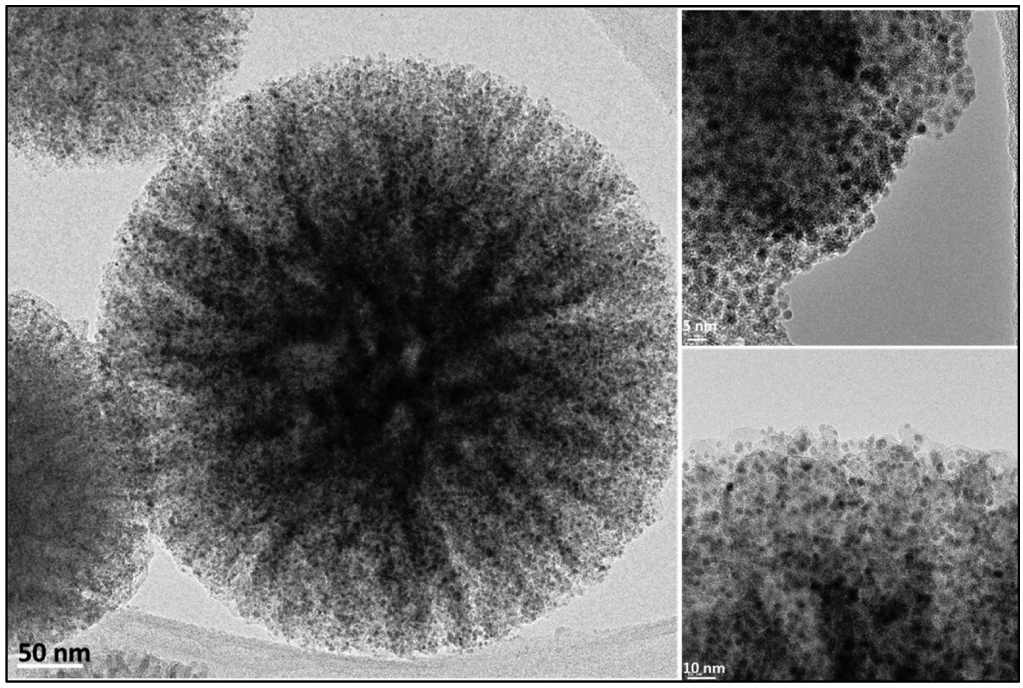

Figure 2. TEM images of KCC-1/Ru nanocatalysts.

angle spinning (CP-MAS) nuclear magnetic resonance (NMR) spectra were recorded at a resonance frequency of 119.23 MHz with 20 kHz spinning rate using a Broadband BB/1H 3.2 mm Bruker CP/MAS probe. The temperature for all experiments was maintained at 298 K. Each spectrum was induced by a nonselective one pulse using the standard one pulseeq program from the Bruker pulse library. To achieve a sufficient signal-to-noise ratio, 2k transients were collected with 30 s recycle delay. Exponential line broadening of 10 Hz applied before Fourier Transformation, and Bruker Topspin 3.0 software was used for data collection and for spectral analysis.

3. RESULTS AND DISCUSSION

3.1. Design and Synthesis of the KCC-1/Ru Nanocatalyst. The first step in synthesizing this catalyst was to functionalize KCC-1 with amino groups, which was achieved by postsynthetic modification of the silica fibers through a reaction with 3-aminopropyltriethoxysilane (KCC-1-NH_2). This material was then treated with $RuCl_3$ followed by hydrogen reduction, to produce Ru nanoparticles supported on KCC-1 (Scheme 1). It is important to note that we were unable to load a detectable amount of Ru on the KCC-1 surface without amine functionalization, as we lost most of $RuCl_3$ during the washing step. When we avoided the washing step, Ru nanoparticles with bigger particle sizes and broad particle size distribution were obtained. However, after amine functionalization, smaller and monodispersed Ru nanoparticles were obtained, indicating the role of amine, which acts as a pseudo ligand and binds with $RuCl_3$. Since we have only 10% grafting of these amino propyl groups, they are well-spaced from each other, which in turns helps the $RuCl_3$ to be uniformly dispersed on the surface of KCC-1 and then in turn the Ru nanoparticles.

3.2. Characterization of the KCC-1/Ru Nanocatalyst. The nanocatalyst KCC-1-NH_2 was then characterized by solid-state ^{29}Si and CP-MAS NMR spectroscopy. The ^{29}Si CP-MAS spectrum (Figure 1a) shows two strong characteristic signals at −99.7 and −109.2 ppm; these signals are assigned to the Q3 and Q4 sites that correspond to the silica substructures with different degrees of condensation. A weak Q2 signal at −90.2 ppm was also observed. The two new signals at −57.3 and −66.8 ppm (absent in KCC-1, Figure 1c) are characteristic of the T2 and T3 sites of $RSiO_3$ units of the as-synthesized silica nanocomposites; these signals indicate the covalent attachment of organic molecules to silica. To confirm that the aminopropyl groups were attached to the KCC-1, a ^{13}C CP-MAS experiment was performed. The resultant spectrum (Figure 1b) exhibited signals at 8.4, 21, and 41.5 ppm that correspond to the three carbon atoms of an aminopropyl group; these signals therefore confirm the presence of this organic functionality. To estimate the amino-group loading, thermo-gravimetric analysis (TGA; Figure 1d) of the KCC-1-NH_2 was conducted under air. After an initial weight loss of water up to 110 °C, the nanocomposite was stable until it reached 350 °C; after which a weight loss of 10.5% was observed up to 650 °C, which can be attributed to the loss of the covalently bound aminopropyl groups. Elemental composition was also determined by CHN analysis, which showed 6.94% carbon, 1.99% hydrogen, and 2.03% nitrogen, confirming the TGA results.

The as-synthesized KCC-1-NH_2 composite was then treated with $RuCl_3$, and Ru(III) was subsequently reduced to Ru(0) using a hydrogen reduction method at 400 °C to produce the KCC-1/Ru nanocatalyst (Scheme 1). TEM analysis of this catalyst revealed that the fibers of KCC-1 were fully loaded with well-dispersed Ru nanoparticles with an average size range of 1−4 nm (Figure 2), which was also confirmed by H_2 chemisorption study (Supporting Information, Figure S1). The X-ray diffraction (XRD) pattern (Supporting Information, Figure S2) contained only peaks from silica support, and no reflections from Ru were observed, because of low metal concentration as well as highly dispersed very small particles. Metal analysis using ICP-OES indicated that as-synthesized catalyst contained 7.11% ruthenium. CHN analysis showed negligible concentration of carbon, hydrogen, and nitrogen,

dx.doi.org/10.1021/cs300179q | ACS Catal. 2012, 2, 1425−1431

which is due to the lesser thermal stability of aminopropyl groups.

3.3. Catalytic Performance of KCC-1/Ru. To investigate the catalytic activity of the KCC-1/Ru nanocatalyst for hydrogenolysis (Scheme 2), propane hydrogenolysis was chosen as a test reaction. Catalytic studies were conducted in fixed-bed dynamic reactor using a propane-hydrogen-helium mixture in the ratio of 1:4:20 at total flow-rate 100 mL/min. To maintain a chemical regime, the catalyst amount was tuned to 200 mg. Initially, the reactions were conducted at different temperatures at atmospheric pressure (Supporting Information, Table S1), and we observed that the reaction proceeded efficiently at 175 °C, so we chose this as the optimal reaction temperature for all further investigations.

Scheme 2. Hydrogenolysis of Alkanes Catalyzed by KCC-1/Ru

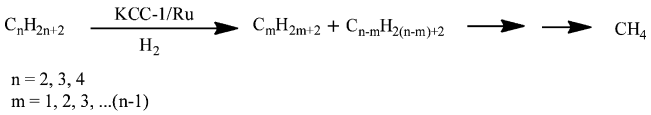

The hydrogenolysis of propane proceeded efficiently with 85−90% conversion (Figure 3a). Methane (selectivity 73%) and Ethane (selectivity 27%) were the major products formed (Figure 3b). After 8 days of the reaction, the cumulative turnover number (TON) was around 13,000.

The regenerability and the lifetime of a catalyst are key factors in the evaluation of the sustainability of any catalytic system. The KCC-1/Ru nanocatalyst was regenerable after the initial run and was active for another 8 days. After regeneration (by treatment with hydrogen at 150 °C for 12 h), we reran the hydrogenolysis of propane and achieved a similar conversion (Figure 4a) and selectivity (Figure 4b) as that of fresh catalyst. To check the stability of the catalyst, the reaction was continued for more than 8 consecutive days (200 h); and minor change in conversion and selectivity was observed, and the catalyst worked as efficiently as like a fresh catalyst during this period with same total cumulative turnover number of 13,000.

To investigate the robustness of this catalyst system, we chose ethane as substrate, which is a challenging feed gas for the hydrogenolysis reaction. Even several good catalytic systems such as highly reactive hydrides of Zr or Hf do not cleave ethane easily.[33,34] The reaction was conducted in a continuous flow fixed-bed reactor. Ethane (2 mL/min) and hydrogen (8 mL/min) were reacted in the presence of the KCC-1/Ru nanocatalyst. To determine the optimal temperature, the reactions were conducted at different temperatures and at atmospheric pressure (Supporting Information, Table S2). We observed that the reaction proceeded efficiently at 250 °C, so we chose this as an optimal temperature for further study.

At 250 °C, ethane hydrogenolysis proceeded efficiently with a 90% conversion, and methane was the only product obtained. The catalyst was fairly stable even after 18 h, and the conversion remained unchanged, which afforded cumulative TON of up to 1000 (Figure 5). The regenerability of the catalyst was also noteworthy. After a first run of the reaction for 18 h, the catalyst was regenerated by treatment with hydrogen at 150 °C for 12 h. The regenerated catalyst exhibited the same activity and stability during the second run of ethane hydrogenolysis under identical reaction conditions. Inductively coupled plasma-optical emissions spectrometry (ICP-OES) analysis of used catalysts showed 7.01% ruthenium concentration, indicating no metal leaching.

Thus, this catalyst system (KCC-1/Ru) exhibited good activity and stability compared with other known catalysts.[1−21] To probe the advantages of fibrous nature of KCC-1 as a support, we prepared this catalyst system using SBA-15 and MCM-41 as support with comparable Ru loading using similar synthesis procedure (Supporting Information, Figures S3 and S4) and then tested for propane hydrogenolysis under identical reaction conditions (Supporting Information, Figures S5 and S6). Table 1 clearly indicates the superiority of the KCC-1/Ru catalyst over SBA-15/Ru and MCM-41/Ru in terms of elevated catalyst activity and high TON.

3.4. Why Does the KCC-1/Ru Nano-Catalyst Show Elevated Catalytic Activity? The effectiveness of nanocatalysts mainly depends on the accessibility of active catalytic sites on the surfaces and in the pores. However, in KCC-1 based catalyst, Ru-nanoparticles are on the fibers and not in the pores like SBA-15 and MCM-41 based catalysts, which enhances their accessibility significantly and in turn improve the activity of the overall catalyst system.

The enhanced activity is also attributable to the effect of the size of Ru nanoparticles. Somorjai and co-workers[35−38] began observing these "size and structure-sensitive" properties of metal-catalyzed reactions in the 1970s and tried to answer one

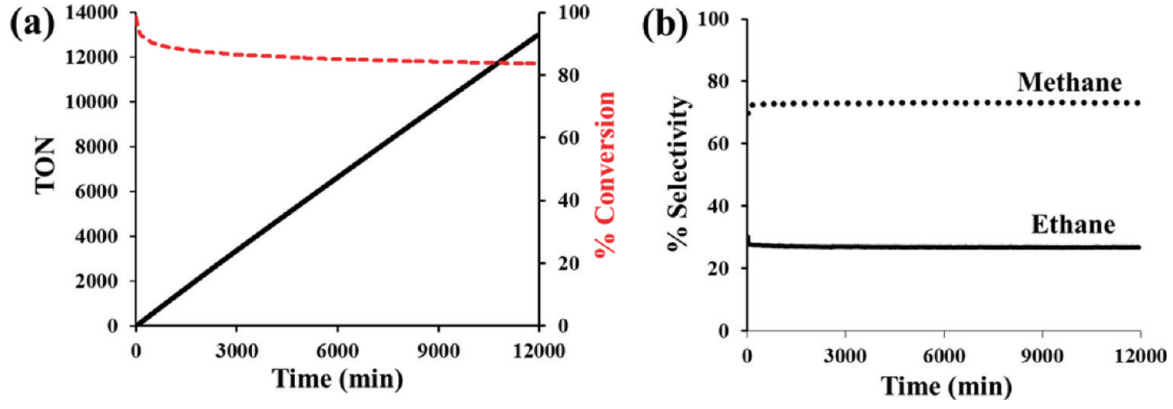

Figure 3. (a) Conversion-turnover number (TON) and (b) selectivity as function of time obtained during the hydrogenolysis of propane catalyzed by KCC-1/Ru in a continuous flow reactor (175 °C, 1 atm) in the presence of hydrogen.

dx.doi.org/10.1021/cs300179q | ACS Catal. 2012, 2, 1425−1431

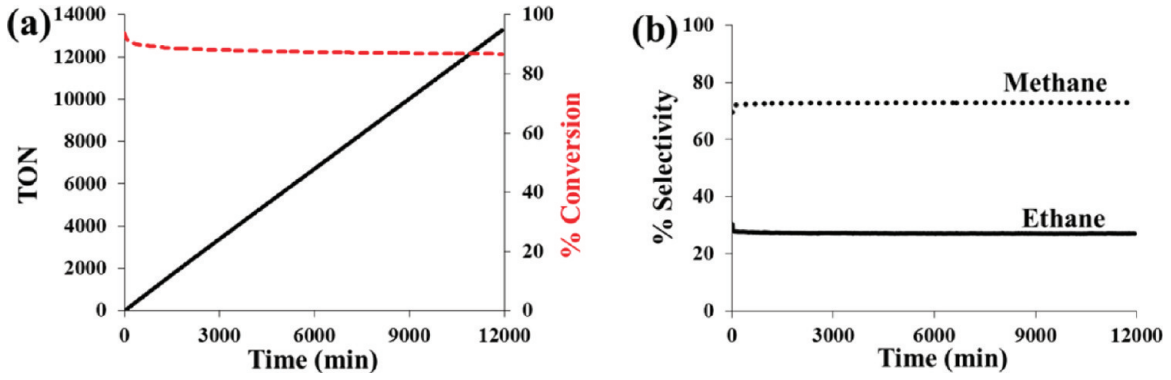

Figure 4. (a) Conversion-turnover number (TON) and (b) selectivity as a function of time obtained during the hydrogenolysis of propane catalyzed by regenerated KCC-1/Ru in a continuous flow reactor (175 °C, 1 atm) in the presence of hydrogen.

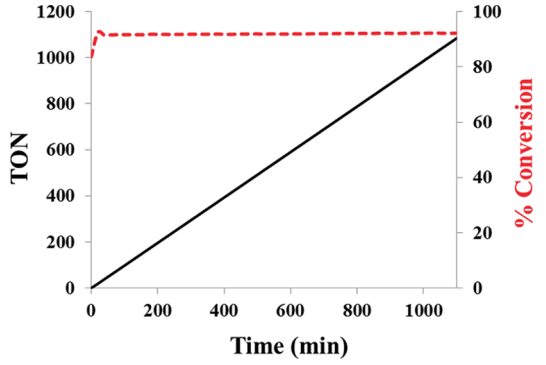

Figure 5. Conversion-turnover number (TON) as a function of time obtained during the hydrogenolysis of ethane catalyzed by KCC-1/Ru in a continuous flow reactor (250 °C, 1 atm) in the presence of hydrogen.

of the key question about the unique properties of these metal nanoparticles. Considering the small size of these metal nanoparticles, the metal atoms occupy crystallographic positions and the crystallites assume shapes such that the nanoparticles possess minimum free energy. The nanoparticles achieve this energy state by forming the maximum number of bonds between all atoms, including surface atoms; this bonding arrangement, in general, leads to nearly spherical nanoparticles. One of the interesting aspects of studies of size-sensitive properties is that this effect is more prevalent in the 1.5 to 5 nm size range. Interestingly, in the case of the KCC-1/Ru catalyst systems, the particle size range (1−4 nm, Figure 2) was well within the active range, and this fact may explain the high catalytic activity of this catalyst system.

In addition to the size, the shape and exposed surfaces of metal nanoparticles can also strongly affect the catalytic properties.[39−43] Somorjai et al. observed that in the case of platinum catalyzed hydrogenolysis, the atomic steps and kinks on the platinum surfaces have striking influences on its activity.[35,36] They identified that atomic steps are primarily responsible for initiating the reaction by C−H and H−H bond breaking while kinks are more active for C−C bond breaking. They have also observed that the hydrogenolysis rate increases with the number of steps and kinks on the catalyst surface. At steps and kink sites, metal atoms possess the lowest coordination number, which makes these atoms catalytically more active. In the case of the KCC-1/Ru catalyst system, close inspection of several TEM images (some are shown in Figure 6) revealed that, in addition to nearly spherical ruthenium

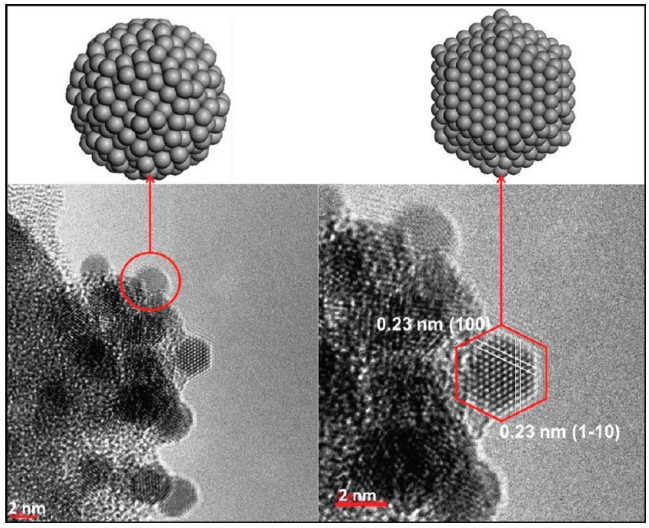

Figure 6. Close view of HRTEM images of KCC-1/Ru nanocatalysts.

nanoparticles, it also contains a fair amount (5−6%) of hexagonal Ru nanoparticles. These hexagonal nanoparticles have several corners and sharp edges (similar to steps and kinks), and the metal atoms at these sites possess the lowest coordination numbers. These more reactive metal atoms at the edges and corners might be helping to enhance the activity of the KCC-1/Ru catalyst system. Such hexagonal Ru nanoparticles were not observed in SBA-15 or MCM-41 based catalysts system under these reaction conditions, which can be due to its tubular pore structure as compared to open fibrous

Table 1. Activity Comparison of KCC-1-/Ru, SBA-15/Ru, and MCM-41/Ru for Propane Hydrogenolysis

catalysts	reaction temperature	conversion (%)	selectivity for CH_4	selectivity for C_2H_6	TON after 7 days
KCC-1/Ru	175 °C	84	73	27	11010
SBA-15/Ru	175 °C	77	73	27	7210
MCM-41/Ru	175 °C	25	86	14	3927

dx.doi.org/10.1021/cs300179q | ACS Catal. 2012, 2, 1425−1431

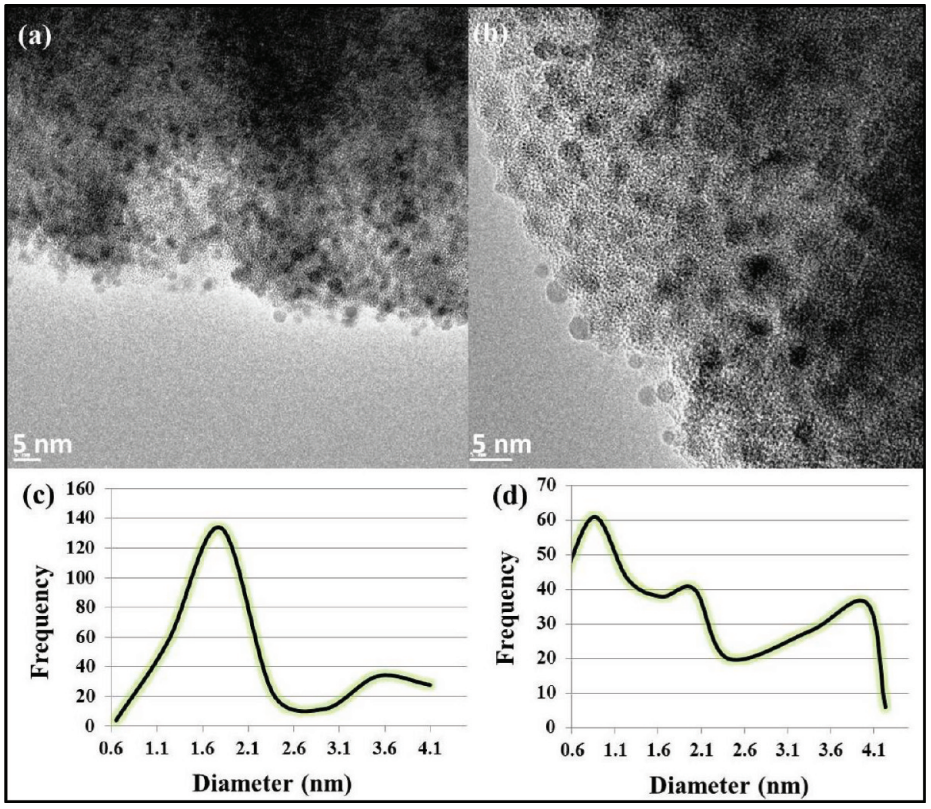

Figure 7. TEM images of KCC-1/Ru nanocatalysts (a) before the reaction and (b) after the reaction. Particle size distribution (c) before the reaction and (d) after the reaction.

structure of KCC-1. We feel that the fibrous nature of KCC-1 plays a role in restricting atomic diffusion in these hexagonal particles, thus confining them to transform to energetically favored spherically shaped particles.

3.5. Why Does the KCC-1/Ru Nano-Catalyst Not Deactivate Even After 8 Days of Reaction? Restricted Ostwald ripening can provide an explanation to this question.[44] The catalytic activity of nano-Ru depends on the size of the particles, with sizes in the range from 1 to 4 nm having been observed to be more effective in catalyzing hydrogenolysis reactions.[35−38] However, these nanoparticles generally lose their activity slowly with reaction time. This loss in activity is a result of the growth of nanoparticles through the Ostwald ripening process, where small nanoparticles merge to form large nanoparticles. Notably, in the case of the KCC-1/Ru catalyst system, we observed minimal Ostwald ripening (Figure 7). Even after 8 days of reaction time, the particle size distribution of the Ru nanoparticles changed from a narrow (1 to 2.6 nm) to a slightly wider (1 to 4.1 nm) range, with an increase in the number of nanoparticles having size greater than 2 nm. Nonetheless, the maximum particle size was still less than 5 nm (Figure 7); therefore, the system maintained nearly the same catalytic activity. The reduced extent of Ostwald ripening may be a consequence of the Ru nanoparticles being situated in between the fibers of KCC-1. The distance within the fibers is a maximum of 5 nm, which means that, even after several days of heating, the nanoparticles cannot grow larger than 5 nm because of the restriction on such growth by the KCC-1 fibers. As the overall particle size remains less than 5 nm, the activity of the nanocatalyst also remains unchanged. These results clearly indicate the advantage of the fibrous nature of KCC-1.

To confirm that restricted Ostwald ripening is due to the fibers, we investigated the locations of Ru nanoparticles in KCC-1/Ru catalyst system by slicing through the KCC-1 spheres and analyzing the inner section using HRTEM and STEM. For this experiment, the KCC-1/Ru was embedded in Epoxy resin and polymerized at 45 °C for 24 h and 62 °C for another 24 h. Ultrathin sections of about 70 nm thickness were cut using a Leica ultramicrotome (EM UC6, Leica Microsystems Inc., Germany). This slice was then mounted on 200 mesh quantifoil copper grids with holey carbon support film (R3.5/1, Quantifoil Micro Tools GmbH, Germany). From HRTEM (Figure 8a, 8c) and STEM (Figure 8b, 8d) of this slice of fresh as well as used catalysts, we can clearly see that most of the Ru nanoparticles are within the fibers of KCC-1. This confirms the role of these fibers in restricting ripening of the nanoparticles.

4. CONCLUSIONS

Fibrous high surface area nanosilica (KCC-1) was amine functionalized and was loaded with ruthenium nanoparticles. TEM images revealed that fibers of KCC-1 were fully loaded with well-dispersed Ru nanoparticles (1−4 nm). The as-synthesized KCC-1/Ru nanocatalyst was then evaluated for the hydrogenolysis of propane and ethane. Catalyst displayed superior activity at atmospheric pressure and low temperatures. The high catalytic activity was due to the highly accessible KCC-1 support as well as formation of Ru-nanoparticles with an active size range (1−4 nm) and the presence of hexagonal-shaped nanoparticles with several corners and sharp edges possessing reactive atoms with lowest coordination numbers. The catalyst was stable with an excellent lifetime and no sign of

dx.doi.org/10.1021/cs300179q | ACS Catal. 2012, 2, 1425−1431

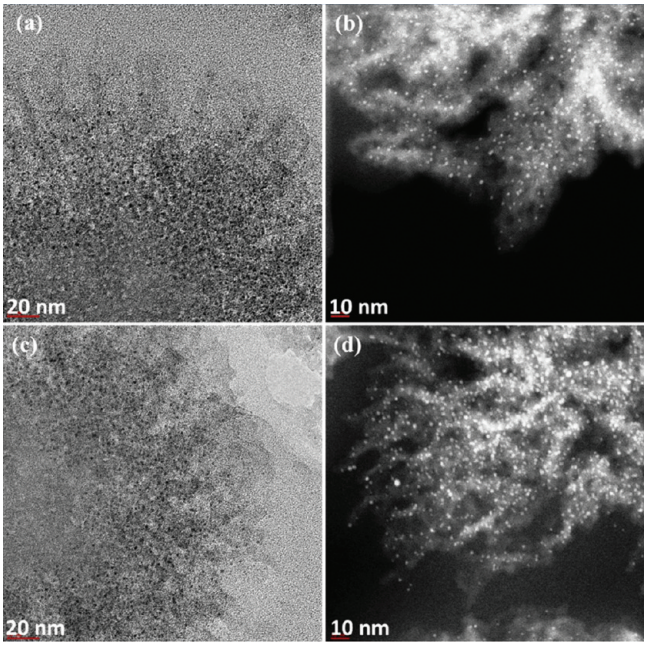

Figure 8. HRTEM and STEM images of the slice of KCC-1/Ru nanocatalysts (a,b) before and (c,d) after the reaction, respectively.

deactivation, even after 8 days. This enhanced stability was possibly due to the restricted Ostwald ripening of nanoparticles.

■ ASSOCIATED CONTENT

Supporting Information

More detailed information about the catalyst material, catalytic tests, and additional information as noted in the text. This material is available free of charge via the Internet at http://pubs.acs.org.

■ AUTHOR INFORMATION

Corresponding Author

*E-mail: vivek.pol@kaust.edu.sa.

Funding

We thank King Abdullah University of Science and Technology (KAUST) for funding and support.

Notes

The authors declare no competing financial interest.

■ REFERENCES

(1) Morikawa, K.; Benedict, W. S.; Taylor, H. S. *J. Am. Chem. Soc.* **1936**, *58*, 1445−1449.
(2) Morikawa, K.; Benedict, W. S.; Taylor, H. S. *J. Am. Chem. Soc.* **1936**, *58*, 1795−1800.
(3) Taylor, E. H.; Taylor, H. S. *J. Am. Chem. Soc.* **1939**, *61*, 503−509.
(4) Sinfelt, J. H. *Catal. Lett.* **1991**, *9*, 159−171.
(5) Sinfelt, J. H. *Catal. Rev.* **1974**, *9*, 147−168.
(6) Sinfelt, J. H. *Adv. Catal.* **1973**, *23*, 91−119.
(7) Sinfelt, J. H. *Catal. Rev.* **1970**, *3*, 175−205.
(8) Bond, G. C.; Hooper, A. D. *Appl. Catal. A: Gen.* **2000**, *191*, 69−81.
(9) Bond, G. C.; Lin, X. *J. Catal.* **1997**, *169*, 76−84.
(10) Rice, R. W.; Keptner, D. C. *Appl. Catal. A: Gen.* **2004**, *262*, 233−239.
(11) Bond, G. C.; Slaa, J. C. *J. Mol. Catal. A: Chem.* **1996**, *106*, 135−149.
(12) Bond, G. C.; Slaa, J. C. *J. Chem. Technol. Biotechnol.* **1996**, *65*, 15−20.
(13) Bond, G. C.; Slaa, J. C. *J. Mol. Catal. A: Chem.* **1995**, *101*, 243−253.
(14) Lomot, D.; Juszczyk, W.; Karpinski, Z.; Larsson, R. *J. Mol. Catal. A: Chem.* **2002**, *186*, 163−172.
(15) Jackson, S. D.; Kelly, G. J.; Webb, G. *J. Catal.* **1998**, *176*, 225−234 , and references numbers 1−5 cited therein.
(16) Sermon, P. A.; Keryou, K. M.; Ahmed, F. *Phys. Chem. Chem. Phys.* **2000**, *2*, 5723−5729.
(17) Engstrom, J. R.; Goodman, D. W.; Weinberg, W. H. *J. Am. Chem. Soc.* **1988**, *110*, 8305−8319.
(18) Martin, G. A.; Dutartre, R.; Yuan, S.; Marquez-Alvarez, C.; Mirodatos, C. *J. Catal.* **1998**, *177*, 105−112.
(19) Roustrup-Nielsen, J. R.; Alstrup, I. *Catal. Today* **1999**, *53*, 311−316.
(20) Rice, R. W.; Keptner, D. C. *Appl. Catal. A: Gen.* **2004**, *262*, 233−239.
(21) Lomot, D.; Juszczyk, W.; Karpinski, Z.; Larsson, R. *J. Mol. Catal. A: Chem.* **2002**, *186*, 163−172.
(22) Polshettiwar, V.; Luque, R.; Fihri, A.; Zhu, H.; Bouhrara, M.; Basset, J.-M. *Chem. Rev.* **2011**, *111*, 3036−3075.
(23) Fihri, A.; Bouhrara, M.; Nekoueishahraki, B.; Basset, J.-M.; Polshettiwar, V. *Chem. Soc. Rev.* **2011**, *40*, 5181−5203.
(24) Polshettiwar, V.; Cha, D.; Zhang, X.; Basset, J.-M. *Angew. Chem., Int. Ed.* **2010**, *49*, 9652−9656.
(25) Polshettiwar, V.; Thivolle-Cazat, J.; Taoufik, M.; Stoffelbach, F.; Norsic, S.; Basset, J.-M. *Angew. Chem., Int. Ed.* **2011**, *50*, 2747−2751.
(26) Fihri, A.; Bouhrara, M.; Cha, D.; Almana, N.; Polshettiwar, V. *ChemSusChem* **2012**, *5*, 85−89.
(27) Polshettiwar, V.; Baruwati, B.; Varma, R. S. *ACS Nano* **2009**, *3*, 728−736.
(28) Nadaguada, M. N.; Polshettiwar, V.; Varma, R. S. *J. Mater. Chem.* **2009**, *19*, 2026−2031.
(29) Polshettiwar, V.; Nadaguada, M. N.; Varma, R. S. *Chem. Commun.* **2008**, 6318−6320.
(30) Polshettiwar, V.; Varma, R. S. *Chem.—Eur. J.* **2009**, *15*, 1582−1586.
(31) Polshettiwar, V.; Baruwati, B.; Varma, R. S. *Chem. Commun.* **2009**, 1837−1839.
(32) Polshettiwar, V.; Baruwati, B.; Varma, R. S. *Green Chem.* **2009**, *11*, 127−131.
(33) Coperet, C.; Chabanas, M.; Saint-Arroman, R. P.; Basset, J.-M. *Angew. Chem., Int. Ed.* **2003**, *42*, 156−181, and references cited therein.
(34) Chabanas, M.; Vidal, V.; Coperet, C.; Thivolle-Cazat, J.; Basset, J.-M. *Angew. Chem., Int. Ed.* **2000**, *39*, 1962−1965.
(35) Khan, D. R.; Petersen, E. E.; Somorjai, G. A. *J. Catal.* **1974**, *34*, 294−306.
(36) Blakely, D. W.; Somorjai, G. A. *J. Catal.* **1976**, *42*, 181−196.
(37) Somorjai, G. A. *Pure Appl. Chem.* **1978**, *50*, 963−969.
(38) Somorjai, G. A. *Adv. Catal.* **1977**, *26*, 1−68.
(39) Ahmadi, T. S.; Wang, Z. L.; Green, T. C.; Henglein, A.; El-Sayed, M. A. *Science* **1996**, *272*, 1924−1925.
(40) Xie, X.; Li, Y.; Liu, Z.-Q.; Hartua, M.; Shem, W. *Nature* **2009**, *458*, 746−749.
(41) Kweskin, S. J.; Rioux, R. M.; Habas, S. E.; Komvopoulos, K.; Yang, P.; Somorjai, G. A. *J. Phys. Chem. B* **2006**, *110*, 15920−15925.
(42) de Smit, E.; Swart, I.; Creemer, J. F.; Hoveling, G. H.; Gilles, M. K.; Tyliszczak, T.; Kooyman, P. J.; Zandbergen, H. W.; Morin, C.; Weckhuysen, B. M.; de Groot, F. M. F. *Nature* **2008**, *456*, 222−225.
(43) Pelzer, K.; Havecker, M.; Boualleg, M.; Candy, J. P.; Basset, J.-M. *Angew. Chem., Int. Ed.* **2011**, *50*, 5170−5173.
(44) Beletskaya, I. P.; Kashin, A. N.; Khotina, I. A.; Khokhlov, A. R. *Synlett* **2008**, 1547−1552.